Optimal MIMO UWB-IR Transceiver for Nakagami-fading and Poisson-Arrivals

Enzo Baccarelli, Mauro Biagi, Cristian Pelizzoni, Nicola Cordeschi
INFO-COM Dept.,"Sapienza" University of Rome , Via Eudossiana 18, 00184 Rome, Italy. Ph. no. +39 06 44585466
FAX no. +39 06 4873300.
Email: {enzobac, biagi, pelcris, cordeschi }@infocom.uniroma1.it

***Abstract*— In this contribution, we develop a (novel) family of Multiple-Input Multiple-Output (MIMO) UWB Impulse-Radio (UWB-IR) transceivers for Orthogonal PPM-modulated (OPPM) coded transmissions over (baseband) multipath-faded MIMO channels. To by-pass expensive channel-estimation procedures, the MIMO channel path-gains are assumed to be *fully unknown* at the receiver. Thus, according to the UWB-IR statistical channel-models currently reported in the literature for both indoor/outdoor application scenarios, we develop and analyze three versions of the resulting noncoherent transceiver, that are optimal for Nakagami, Gaussian, and Log-normal distributed channel-gains, respectively. As dictated by the Saleh-Valenzuela (SV) UWB model, the resulting noncoherent Maximum-Likelihood (ML) Decoder *explicitly* accounts for the Poisson-distribution of the path-arrivals. Hence, after analytically evaluating the performance of the proposed noncoherent transceiver via suitable versions of the Union-Chernoff bound, we prove that the family of Space-Time OPPM (STOPPM) recently presented in the Literature is able to attain *full-diversity* in the considered multipath-affected application scenario. To corroborate the carried out performance analysis, we report several numerical results supporting *both* the medium/long coverage ranges attained by the proposed STOPPM-coded noncoherent transceiver, and its performance robustness against the degrading effects induced by Inter-Pulse-Interference (IPI), spatially-correlated multipath fading and mistiming.**

***Index Terms*— Dense-Multipath, UWB-IR MIMO channels, Space-Time Blocks Codes (STBCs), STOPPM codes, Poisson-distributed arrivals, noncoherent Space-Time decoding, IPI.**

I. INTRODUCTION

Ultra-Wide-Band-Impulse Radio (UWB-IR) is an emerging wireless technology proposed for low-power high-speed data communication over unlicensed bandwidth spanning several GHz [1,13]. Up to date, due to hard limits on the radiated power levels, this technology is devised *mainly* for short-range indoor applications in WPAN environments (see the proposals of IEEE 802.15.3 and IEEE 802.15.4 Working Groups, [29]). As a consequence, the UWB-IR Physical Layer is designed to provide data rates of about 110 Mbps, 200 Mbps and (optionally) 480 Mbps at 20mt, 10mt and 2-3mt, respectively ([13, Chap.10], [36]). So, till now, UWB-IR is essentially considered as a competitor of the Bluetooth one. However, due to the (very) large bandwidth and angular spread spanned by the UWB-IR signals, several measurement campaigns on the UWB-IR channels unveiled the high *spatio-temporal* diversity that the UWB-IR channels are, in principle, able to offer, ([15,20,21], [13, Chap.3]). This has motivated some recent works [28,29] in trying to extend UWB-IR technology toward 4G-WLAN-compliant operating scenarios. To meet this goal and (fully) exploit *both* spatial and temporal diversity, new simple-to-implement radio transceiver architectures, combining the *MIMO paradigm* with the *UWB-IR one*, should be envisioned for low-power medium/long-range (possibly) outdoor applications.

A. Previous Contributions

Current research on MIMO UWB-IR systems *mainly* focuses on flat-faded (e.g., frequency-nonselective) application environments. Specifically, in [7] the performance of MIMO UWB-IR systems over Gaussian flat-faded channels is analyzed by simulations, while in [11,12] Alamouti-like STBCs codes are proposed for Gaussian and Nakagami flat-faded channels under the (somewhat optimistic) assumption of Perfect Channel State Information (PCSI) at the receiver. The recent contribution in [31] presents lower bounds on the SNRs required by multi-rate UWB-IR systems operating over flat-faded channels.

The statistical features of the spatio-temporal multipath fading which result from MIMO UWB-IR channels have been also taken into account and exploited, but to make the analysis and design of the proposed transceiver more tractable, several (somewhat unrealistic) simplifications have been introduced. Most of them are mainly related to the fact that the arrival-times of the channel-paths are considered to be evenly time-spaced [19] while, according to several measurement campaigns (see [6], [13] and references therein), path arrivals are, indeed, clusterized, as captured by the Saleh-Valenzuela (SV) model [9]. Moreover, path-gains of (indoor) UWB channels typically follow a Log-normal distribution, that is quite difficult to analytically tackle [5,26]. As a consequence, the Log-normal distribution is often (coarsely) approximated by the Gaussian one. This is done, for example, in [2], where an analog version of the Alamouti-code is developed for UWB-IR systems affected by multipath Gaussian fading with evenly-spaced arrival-times. Under the same

This work has been developed under the Italian Project: "Wireless 802.16 Multi-antenna mEsh Networks (WOMEN)" under grant number 2005093248, and partially presented at IEEE ICC'07.

assumptions, in [18] a comparative performance analysis of Time-Hopping-vs- Direct Sequence Spread Spectrum MIMO UWB-IR transceivers is carried out, for *uncoded* BPSK modulated data transmissions. In [30], the Inter-Symbol-Interference (ISI) effects induced by the evenly-spaced multipath-spread is accounted for by proposing and comparing some equalization procedures. The main drawbacks of such approach are the high cost requested to implement the equalizers [26, Chap.11], and the large processing times needed to update the estimations of the high number of channel paths composing the MIMO UWB-IR links.

Overall, up to date, an analytical approach to deal with Log-normal distributed multipath fading seems to be developed (only) in [3]. However, the analysis in [3] focuses on MIMO UWB-IR transceiver for *uncoded* BPSK-modulated communications and it limits to consider a (somewhat sub-optimal) receiving architecture composed by a Zero Forcing equalizer cascaded to a Rake-combiner equipped with equally-spaced taps. The assumption of evenly spaced arrival-times is still retained in [12], where several sub-optimal transceiver architectures for UWB-IR propagation environments affected by Nakagami-distributed fading are proposed and tested. Overall, to the best of Authors' knowledge, the clustering effect of the SV model is accounted for in [24], where a MIMO UWB system is proposed for *uncoded* PPM. However, the transceiver in [24] is not able to fully exploit the spatial-diversity offered by the underlying MIMO UWB channel, as pointed out in [13, Chap.3].

B. Proposed Contributions and Organization of the Work

Motivated by the above overview, in this contribution we develop, analyze and test a novel noncoherent transceiver which is able to *fully-exploit* the spatio-temporal diversity offered by the underlying MIMO UWB-IR multipath channels, *without requiring* any channel-estimation procedure. To attain full-diversity gain in multipath-affected application scenarios with Poisson-distributed path-arrivals, the proposed transceiver capitalizes the performance improvements offered by the family of OPPM-based variable-rate unitary STBCs (namely, the STOPPM codes) recently proposed in [4]. Specifically, main contributions on this work may be so summarized.

- First, we develop a (novel) family of MIMO UWB-IR transceiver for the noncoherent ML detection of OPPM-data transmitted over multipath-channels with Poisson-distributed path arrivals. As dictated by the current statistical channel-models [13], the cases of Nakagami-distributed path gains is considered. Due to many (differently-scattered) environments on which UWB-IR solutions are currently proposed [5], the optimal versions of the MIMO transceiver for Gaussian and Log-normal-distributed path-gains are reported too.
- Second, after deriving the corresponding Union-Chernoff bounds on the performance of the resulting ML noncoherent transceivers, we show that, under (quite mild) assumptions about the system operating conditions, the STOPPM codes recently proposed in [4] are able to attain maximum spatio-temporal diversity.
- Third, we prove that, due to the Poisson-distribution of the path-arrivals, the average BER performances of the optimized transceivers *do not vanish* at high SNRs. They approach, indeed, a BER floor, whose value exponentially decays with the average number of channel-paths received over a signalling period.
- Fourth, we report several numerical results supporting the medium/long coverage range achieved by the proposed transceivers in typical UWB-IR multipath-faded application environments.
- Finally, we test the performance robustness of the proposed transceivers against channel-impairments induced by Inter-Pulse-Interference (IPI), spatially-correlated fading, and mistiming.

The rest of this contribution is organized as follows. After introducing in Sect.II the considered system model, in Sect.III we derive the overall architecture of the proposed transceiver. Thus, after (shortly) re-visiting in Sect.IV the main properties of the STOPPM codes, in Sect.V we develop the corresponding noncoherent ML decoders for Nakagami, Gaussian and Log-normal-distributed channel-gains. Numerical results testing actual performance of the proposed transceiver are presented in Sect.VII, both in terms of BER-v.s.-SNR and attained coverage-ranges. Finally, some conclusions and hints for future research are drawn in Sect.VIII. Proofs of the main results are reported in the final Appendices.

Before proceeding, let us spend few words about the adopted notation. Specifically, in the sequel, bold capital letters denote matrices, bold and underlined symbols indicate vectors, while non-bold characters are used for scalar quantities. Furthermore, $(.)^T$ means transposition, $\ln(.)$ indicates natural logarithm, $\cosh(.)$ and sech$(.)$ stand for hyperbolic cosine and secant, det[$\mathbf{A}$] is the determinant of the matrix $\mathbf{A}$, $\mathbf{I}_L$ is the (L×L) identity matrix, $\underline{\mathbf{1}}_m$ is the (m×1) column vector with all one-entries, $\underline{\mathbf{0}}_m$ is the (m×1) null vector, while $\mathbf{0}_L$ is the (L×L) null matrix.

II. THE CONSIDERED SYSTEM MODEL

The baseband point-to-point link we consider in Fig.1 is composed by N_t-transmit and N_r-receive antennas working on an UWB-IR MIMO channel. At the signalling period $T_s(sec.)$, the (memoryless) source of Fig.1 generates an L-ary ($L \geq 2$) information symbol $b \in \{0, 1, ..., L-1\}$. The Multi-Antenna transmitter maps b onto N_t OPPM M-ary baseband analog signals $\left\{x^{(i)}(t), 1 \leq i \leq N_t\right\}$ of time-duration limited up to T_s, according to the following relationship:

$$x^{(i)}(t) \triangleq \sum_{m=0}^{N_f-1} \sqrt{\frac{E_f}{N_t}} p(t - mT_f - d_i T_p),$$

$$0 \leq i \leq N_t \ , 0 \leq t \leq T_s, \quad (1)$$

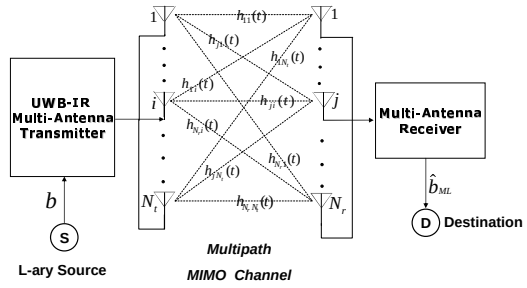

Figure 1. The considered MIMO point-to-point UWB-IR system with N_t-transmit and N_r-receive antennas. The Multi-Antenna transmitter is employed for the ST coding of the L-ary symbol b. The MIMO UWB-IR channel is affected by multipath fading and it is described by $(N_t \times N_r)$ baseband impulse channel-responses $\{h_{ji}(t),\ 0 \le i \le N_t,\ 0 \le j \le N_r\}$.

where $d_i \in \{0, ..., M-1\}$ is the M-ary ($M \ge 2$) PPM symbol radiated by the i-th transmit antenna over the signalling period T_s. The (unit-energy) UWB baseband pulse $p(t)$ in (1) is limited up to $T_p(sec.)$, and it is repeated N_f times over each signalling period T_s [1]. Hence, since each signalling period is partitioned into N_f no overlapped frames of duration $T_f(sec.)$, then T_s must be set as the product $N_f T_f$. Furthermore, to avoid Inter-Frame Interference (IFI), T_f must exceed the UWB channel delay-spread T_μ, whose typical values are given in Table I for outdoor application scenarios [5, Table III], [6, Table II]. Hence, in the sequel we set T_f as $MT_p + T_\mu$.

UWB Channel Models (CM)	λ $[1/ns]$	γ $[ns]$	T_μ $[ns]$
CM5	2.41	3.7	5.5
CM6	1.13	9.3	15.9

TABLE I.
SINGLE-INPUT SINGLE-OUTPUT (SISO) UWB-IR CHANNEL MODELS RECOMMENDED BY IEEE 802.15.4A WG (SEE TABLE III OF [5]).

Finally, E_f *(Joule)* in (1) denotes the energy globally spent by the N_t transmit antennas over each frame-period.

A. MIMO UWB-IR Channel Modeling and Fading Statistics

Due to the very low time-duration of the adopted pulse $p(.)$ in (1), UWB communications are typically affected by frequency-selective fading phenomena that scatter the energy of the received signal over a (very large) number of (resolvable) paths. Thus, after indicating by $h_{ji}(t)$ the baseband real-valued analog impulse-response of the SISO link from the i-th transmit antenna to the j-th receive one, as in eq.(1) of [8] we may collect these impulse-responses into the corresponding $(N_t \times N_r)$ matrix $\mathbf{H}(t)$, thereinafter referred as the MIMO channel impulse-response matrix [8]. The IEEE 802.15.3a and IEEE 802.15.4a Workgroups recommend that, at least for highly-scattered (indoor) applications, each SISO impulse-response $h_{ji}(t)$ in Fig.1 is modelled as the superposition of several path-clusters, with both inter-cluster and intra-cluster inter-arrival times being exponentially distributed [5,9]. However, at least for outdoor medium-range applications, it has been experienced that the paths composing the first cluster are the strongest ones [13, Chap.3], [17], so that a "Single-Cluster Poisson Model" suffices for capturing the behavior of each $h_{ji}(t)$. Thus, according to this model, $h_{ji}(t)$ may be expressed as [13, Chap.3][1]

$$h_{ji}(t) \triangleq \sum_{n=0}^{V} h_n(j,i)\delta\left(t-\tau_n\right) \equiv \sum_{n=0}^{V} \beta_n(j,i)\alpha_n(j,i)\delta\left(t-\tau_n\right), \quad 1 \le i \le N_t,\ 1 \le j \le N_r. \quad (2)$$

In (2), the (integer-valued) number V of received paths over a signalling period T_s is a Poisson-distributed random variable (r.v.) with mean value $\mathrm{E}\{V\} \equiv \lambda T_s$ (see Table I), while $\tau_n(ns)$ is the (non-negative) arrival-time of the n-th path[2]. Furthermore, the (real-valued) r.v. $h_n(j,i)$ in (2) is the n-th path gain of (SISO) link going from the i-th transmit antenna to the j-th receive one (see Fig.1), while the binary r.v. $\beta_n(j,i) \in \{-1,1\}$ and the (non-negative) r.v. $\alpha_n(j,i)$ in (2) are the corresponding phase (e.g., the sign of $h_n(j,i)$) and amplitude, respectively.

About the statistic (e.g., the probability density function (pdf)) of the channel coefficients $\{h_n(j,i)\}$, it is, indeed, application depending [13, Chaps.1,3], [2,3,11,12]. Some (recent) measurement campaigns point out that the statistic of the fading affecting rich-scattered medium-range quasi-LOS UWB-IR links may be well modeled by resorting to the (more versatile) Nakagami pdf [12], [13, Chap.3], while Log-normal distributed channel amplitudes $\{\alpha_n(j,i)\}$ may be more suitable for less scattered LOS short-range indoor propagation environments and, indeed, the Log-normal distribution is recommended by IEEE 802.15.3a and IEEE 802.15.4a Workgroups for WPAN and sensor applications [5,13]. Finally, argumentations based on the Central Limit Theorem [2,5,10,16] support the conclusion that zero-mean *Gaussian distributed* channel-coefficients well model highly-scattered outdoor NLOS propagation environments, where each received path in (2) is, indeed, the superposition of several equal-strength scattered components. Hence, since, in principle, the transceiver we develop should be able to operate in short/medium/long-range indoor/outdor LOS/NLOS environments, in this contribution we consider *all* the above

[1]The generalization of the architecture of the proposed transceiver to the more general "Multiple-Cluster Poisson Model" is quite direct and, by fact, it only requires the adoption of somewhat more complex analytical notations.

[2]In the sequel, we assume that $\tau_n > \tau_{n-1}$, so that, according to [9], the n-th inter-arrival time $\Delta_n \triangleq (\tau_n - \tau_{n-1})$ is an exponentially-distributed non-negative r.v. Furthermore, since the r.v. V is assumed to be Poisson-distributed, we have: $P\left(V=k\right) = e^{-\lambda T_s}\frac{(\lambda T_s)^k}{k!}$, $k = 0, 1, 2...$ This means that the probability $P\left(V=0\right)$ to receive no paths over a signalling period *does not vanish*, but it equates $e^{-\lambda T_s}$.

mentioned pdfs, and then we derive and analyze the optimal versions of the proposed noncoherent MIMO UWB-IR transceiver for Nakagami, Gaussian and Log-normal-distributed fading. In doing so, we are also able to evaluate the effects induced by the fading statistics on the ultimate performance (e.g., diversity and coding gain) of the proposed transceiver.

B. Received Signals and Inter-Pulse-Interference (IPI)

Under the assumption of perfect time-alignment at the receiver (e.g., the arrival times $\{\tau_n\}$ in (2) are perfectly estimated at the receiver), the (analog real-valued baseband) signal $y_j(t)$ measured at the output of the j-th receive antenna may be expressed via the following convolution:

$$\begin{aligned} y_j(t) &= \sum_{i=1}^{N_t} x^{(i)}(t) \circledast h_{ji}(t) + w_j(t) \\ &\stackrel{(a)}{\equiv} \sum_{i=1}^{N_t}\sum_{n=0}^{V} h_n(j,i)x^{(i)}(t-\tau_n) + w_j(t), \\ &\equiv \sum_{i=1}^{N_t}\sum_{n=0}^{V}\sum_{j=1}^{N_f} h_n(j,i)\sqrt{\frac{E_f}{N_t}}p(t-mT_f-d_iT_p-\tau_n) + w_j(t), \\ & \qquad\qquad 1 \le j \le N_r, \quad (3) \end{aligned}$$

where $w_j(t)$ is the real-valued zero-mean white Gaussian noise with unit two-side power-spectral density impairing the signal received by the j-th antenna, $\circledast$ is the convolution operator and (a) stems from the channel model in (2). Before proceeding, let us spend few words about the IPI effects (possibly) induced by the multipath-spread of the UWB channel. After denoting by $\rho(t) \triangleq p(t) \circledast p(-t)$ the autocorrelation function of the pulse in (1), in order to *retain* the orthogonality property of the employed PPM format *also* at the receiver side, we are forced to assume that the following relationship holds (see the last row of eq.(3)):

$$\rho\Big((l-m)T_p + (\tau_f - \tau_q)\Big) \triangleq$$

$$\int_{-\infty}^{+\infty} p(t-mT_p-\tau_f)p(t-lT_p-\tau_q) \equiv \delta_{l,m}\delta_{f,q}, \quad (4)$$

where $\delta_{l,m}$ and $\delta_{f,q}$ are the Kronecker's deltas. However, the adopted Poisson channel model dictates that the inter-arrival times $\Big\{\Delta_n \triangleq \tau_n - \tau_{n-1}\Big\}$ are exponentially distributed r.v.s, so that, in principle, each Δ_n may assume very large (even unbounded) values. In turn, this means that the IPI-free operating condition in (4) may be guaranteed *only* in a statistical sense, for example, over a fraction (e.g., percentage) $\eta \in (0,1)$ of the overall working (e.g., service) time of the system. Thus, motivated by the above consideration, in the sequel we assume that the time-duration T_p of the pulse $p(t)$ in (1) meets the following bound:

$$T_p \le -\ln(\eta)/\lambda M, \quad (5)$$

that, in turn, guarantees that the IPI-free operating condition in (4) is met at least over a fraction η of the overall working time of the system. We anticipate that the assumption of IPI-free operating conditions will be relaxed in Sect.VII, where we numerically test the performance loss induced by small values of η.

C. Some refinements and additional considerations about the adopted MIMO UWB-IR channel model

Before proceeding, we want to detail some refinements and explicative comments about the here considered communication model.

To begin with, let us remark that the channel coefficients $\{h_n(j,i)\}$ in (2), (3) *do not depend* on the time-index t, thus meaning that $\{h_n(j,i)\}$ are assumed to be time-invariant over (at least) a signalling period T_s. By fact, the assumption of quasi-static fading may be considered well met when the coherence time $T_{coh}(ns)$ of the MIMO channel in (3) equates (at least) the signalling period T_s, e.g.,

$$T_{coh} \ge T_s = N_f T_f \equiv N_f(MT_p + T_\mu). \quad (6)$$

Since typical systems work at $N_f \le 10$ and $T_f \le 30(ns)$, the above inequality may be considered met when T_{coh} exceeds $250 - 300(ns)$. Coherence times of this order are quite typical for 4GWLAN systems serving nomadic users [6,13,22].

Next, in order to by-pass expensive channel-estimation procedures, the receiver of Fig.1 is *fully unaware* about the actual values retained by the channel-coefficients $\{h_n(j,i)\}$ over each signalling period (e.g., No Channel State Information (NCSI) is available at the receiver), so that it must perform noncoherent detection of the transmitted (coded) data.

Furthermore, in the sequel we also assume that the channel coefficients $\{h_n(j,i)\}$ are *uncorrelated* over both delay-index n and spatial-indexes (j,i), thus meaning that the scattering induced by fading is assumed to be uncorrelated over *both* time and spatial dimensions. Although it is experienced that time-uncorrelated scattering is a quite typical operating condition in NLOS medium/long-range outdoor applications [13, Chap.3], the assumption of spatially uncorrelated fading may be, in principle, more questionable. In this regard, we point out that several measurements of indoor/outdoor MIMO UWB-IR links [13, Sect.3.5] lead to the conclusion that the spatial-correlation exhibited by MIMO UWB-IR channels is typically low and, indeed, may be neglected at all when the transmit/receive antennas are spaced apart of $\lambda/2$, where λ is the wavelength of the radiated signals in (1) evaluated at the peak-frequency of the corresponding spectra [13, Chap.3]. However, since, in principle, high spatial-correlations may induce no negligible performance loss, we anticipate that the assumption of spatially uncorrelated fading is relaxed in Sect.VII, where we test the performance of the proposed transceiver in the presence of (highly) spatially-correlated channel-gains.

According to the MIMO channel models for wideband applications developed in [8], the path-delays $\{\tau_n\}$ in

(2) are assumed to be independent from the spatial-indexes (j,i) of the transmit/receive antennas. As pointed out in [8], this assumption is well met especially in medium/long-range 4GWLAN application scenarios, where the delays induced by the spatial-dimensions of the transmit/receive antenna arrays are negligible with respect to those induced by the multipath propagation across the physical channel. For the same reason, in the sequel we assume that the Multipath Intensity Profiles (MIPs) of the SISO links in (2) do not depend on the spatial-indexes (j,i), but only on the delay-index τ_n, so that we pose: $\sigma_n^2 \equiv \mathrm{E}\left\{h_n^2(j,i)\right\}$.

About the (quite critical) assumption of perfect synchronization (e.g., perfect information at the receiver about the path-delays $\{\tau_n\}$) previously introduced at the beginning of Sect.II-B, we anticipate that it is relaxed in Sect.VII, where we test the performance robustness of the proposed transceiver against mistiming effects. The overall topic of time-acquisition and tracking is afforded in [25] and in [28, Chap.7] for MIMO UWB-IR channels affected by flat and frequency-selective fading, respectively.

Lastly, we remark that, since the number V of received paths in (2), (3) is modelled as Poisson-distributed r.v., thus V may assume very large (in principle, even unbounded) values. However, we point out that, in practice, the maximum number N_{max} of paths resolved by the receiver is finite and limited up to $N_{max} = \lfloor \frac{T_\mu}{T_p} \rfloor$, with $\lfloor . \rfloor$ denoting the floor operator.

III. Front-end Processing and Decision Statistics

The ultimate task of the receiver depicted in Fig.1 is to compute the ML decision $\hat{b}_{ML}$ on the information symbol b by exploiting the analog signals in (3) observed at the outputs of the receive antennas over the current signalling period. For this purpose, let us note that the following outputs of filters matched to the (multipath-delayed) versions of the M-ary OPPM pulses

$$y_j(l,n) \triangleq \frac{1}{\sqrt{N_f}} \int_0^{T_s} y_j(t) \left[\sum_{k=0}^{N_f-1} p(t - kT_f - lT_p - \tau_n) \right] dt, \quad 0 \le l \le M-1, \quad (7)$$

constitute a discrete set of $(M \times (V+1) \times N_r)$ statistics that are *sufficient* for the ML detection of the transmitted information symbol (see [23] for additional details on this topic). Thus, after replacing $y_j(t)$ in (7) by its definitory relationship in (3), an exploitation of the orthogonality property in (4) allows us to develop (7) as follows:

$$y_j(l,n) = \sqrt{\frac{\gamma_b N_f \lg_2 L}{N_t}} \sum_{i=1}^{N_t} h_n(j,i)\phi_i(l) + w_j(l,n) \equiv \beta \sum_{i=1}^{N_t} h_n(j,i)\phi_i(l) + w_j(l,n), \quad (8)$$

where $\gamma_b \triangleq \frac{2E_f}{N_0 \lg_2 L} \equiv \frac{E_f}{\lg_2 L}$, is the SNR per transmitted information bit. Furthermore, the terms $\{\phi_i(l)\}$ in (8) depend on the transmitted information symbol $b = l$ according to[3]

$$\phi_i(l) \triangleq \frac{1}{N_f} \sum_{k=0}^{N_f-1} \cdot \int_0^{T_s} p(t - kT_f - d_i T_p - \tau_n) p(t - kT_f - lT_p - \tau_n) dt \equiv \begin{cases} 1, \text{ for } d_i = l \\ 0, \text{ for } d_i \neq l \end{cases} \quad (9)$$

while the noise terms

$$w_j(l,n) \triangleq \frac{1}{\sqrt{N_f}} \sum_{k=0}^{N_f-1} \int_0^{T_s} w_j(t) p(t - kT_f - lT_p - \tau_n) dt, \quad (10)$$

in (8) are real-valued mutually-uncorrelated zero-mean unit-variance r.v.s. Therefore, after indicating by $\mathbf{Y}_j$, $1 \le j \le N_r$, the $(M \times V)$ matrix collecting the statistics $\{y_j(l,n),\ 0 \le l \le M-1,\quad 0 \le n \le V\}$ in (8), we may recast the relationships in (8) in the following (compact) matrix form:

$$\mathbf{Y} \triangleq [\mathbf{Y}_1 \ ... \ \mathbf{Y}_{N_r}] \equiv \beta \mathbf{\Phi} \mathbf{H} + \mathbf{W}, \quad (11)$$

where the $(M \times N_r(V+1))$ matrix $\mathbf{Y}$ collects the observation statistics in (8), while the $(M \times N_r(V+1))$ matrix $\mathbf{W}$ is for all the noise terms in (10). Furthermore, $\mathbf{H} \triangleq [\mathbf{H}_0 \ldots \mathbf{H}_V]$ in (11) is the $(N_t \times N_r(V+1))$ channel matrix obtained by the ordered stacking of the matrices $\{\mathbf{H}_n,\ 0 \le n \le V\}$, where, in turn, $\mathbf{H}_n$ is the $(N_t \times N_r)$ matrix built up by the channel-gains $\{h_n(j,i),\ 1 \le i \le N_t,\ 1 \le j \le N_r\}$ of the n-th path. Finally, $\mathbf{\Phi}$ in (11) denotes the $(M \times N_t)$ matrix composed by the binary-valued $\{\phi_i(l)\}$ coefficients in (9). Specifically, $\mathbf{\Phi}$ represents the space-time matrix codeword associated to the (ordered) N_t-ple $\{d_1, ..., d_{N_t}\}$ of M-ary OPPM data radiated by the transmit antennas over the current signalling period (see eq.(1)).

IV. A brief review on the STOPPM codes and their main Properties

Since the Multi-Antenna transmitter of Fig.1 maps each value l assumed by the information symbol b into the corresponding (matrix) value $\mathbf{\Phi}_l$ assumed by the transmitted space-time codeword $\mathbf{\Phi}$, thus, from a statistical point of view, $\mathbf{\Phi}$ in (11) is an L-ary r.v. whose (matrix) outcomes $\{\mathbf{\Phi}_l,\ 0 \le l \le L-1\}$ are equiprobable and constitute the codewords of the adopted STBC. Furthermore, the relationship in (9) forces the N_t column of $\mathbf{\Phi}_l$ to be *unit-vectors* of $\mathbb{R}^M$, that is,

$$\mathbf{\Phi}_l \equiv \left[\underline{\mathbf{e}}_1^{(l)} \ldots \underline{\mathbf{e}}_{N_t}^{(l)} \right] \leftrightarrow b = l, \quad 0 \le l \le L-1, \quad (12)$$

where the ordered sequence of N_t unit-vectors of $\mathbb{R}^M$ in $\mathbf{\Phi}_l$ depends on the value l actually assumed by the

[3] After recalling that d_i in (9) is the M-ary OPPM data radiated by the i-th transmit antenna, from (4) it arises that the integral in (9) is unit for $d_i = l$, while it vanishes when $d_i \neq l$.

transmitted information symbol b. Furthermore, since in [32] it is proved that *unitary* STBCs optimize the transmission performance of fading-affected MIMO channel when *non-coherent* detection is carried out at the receiver side, thus, without loss of optimality, in the next Sections we directly assumes that $\mathbf{\Phi}$ in (11) is the matrix codeword of an *unitary* STBC.

A. STOPPM codes

In this respect, STOPPM codes introduced in [4] are a (particular) class of variable-rate OPPM-based unitary STBCs characterized by the following two definitory properties:

i) the size M of the employed OPPM format equates LN_t, that is,

$$M = LN_t; \tag{13}$$

ii) the N_t columns of the l-th matrix codeword $\mathbf{\Phi}_l$ are constituted by the N_t unit-vectors of $\mathbb{R}^M$ with index i ranging from $i = lN_t$ to $i = \big((l+1)N_t\big) - 1$, that is

$$\mathbf{\Phi}_l \triangleq \Big[\underline{\mathbf{e}}(lN_t) \ \ldots \ \underline{\mathbf{e}}((l+1)N_t - 1)\Big], \ \ 0 \le l \le L-1. \tag{14}$$

Directly from the above definition, it follows some interesting properties of the STOPPM codes we go to list (see [4] for additional details and formal proofs).

First, STOPPM codes are *orthogonal and unitary* STBCs, thus meaning that

$$\mathbf{\Phi}_l^T \mathbf{\Phi}_m = \mathbf{0}, \ \text{ for } \ l \neq m, \ \text{ and}$$

$$\mathbf{\Phi}_l^T \mathbf{\Phi}_l = \mathbf{I}_{N_t}, \ \text{ for any } \ l. \tag{15}$$

Second, STOPPM codes constitute a family of variable-rate STBCs, with spectral efficiency $\eta_{STOPPM}(bit/sec/Hz)$ given by (see eq.(13))

$$\eta_{STOPPM} = \lg_2(M/N_t)/MN_f, \quad (bit/sec/Hz). \tag{16}$$

Finally, being STOPPM codes unitary and orthogonal, the Bit-Error-Probability $P_E^{(b)}$ of a STOPPM code is directly related to the corresponding Word Error Probability (WEP) $P_E \triangleq P\left(\mathbf{\Phi} \neq \widehat{\mathbf{\Phi}}_{ML}\right)$ via the following relationship:

$$P_E^{(b)} = \left(\frac{L}{2(L-1)}\right) P_E. \tag{17}$$

V. The proposed Noncoherent ML Decoder for Nakagami, Gaussian and Log-normal-distributed multipath fading

Since the $(M \times N_r(V+1))$ observation matrix $\mathbf{Y}$ in (11) is a sufficient statistic for the ML detection of the transmitted symbol b and, in addition, each information symbol $b = l$ is one-to-one mapped into the corresponding matrix codeword $\mathbf{\Phi}_l$ of the employed STOPPM code (see eq.(12)), the decision rule implemented by the ML detector of Fig.2 may be directly expressed as

$$\hat{\mathbf{\Phi}}_{ML} = \underset{0 \le l \le L-1}{\arg\max} \left\{ p\left(\mathbf{Y} \mid \mathbf{\Phi}_l\right) \right\}, \tag{18}$$

where $p(. \mid .)$ in (18) is the pdf of $\mathbf{Y}$ conditioned on the l-th codeword $\mathbf{\Phi}_l$. In the Appendix A is proved that,

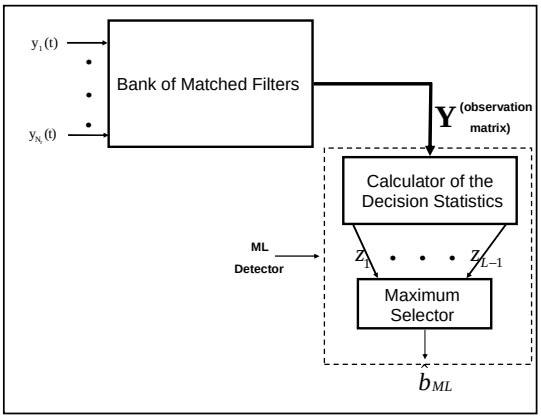

Figure 2. A block-scheme of the proposed Multi-Antenna noncoherent receiver .

regardless from the pdf adopted to model the channel coefficients $\{h_n(j,i)\}$, the ML decision rule in (18) can be equivalently rewritten in terms of L suitable real-valued decision statistics $\{z_l, \ l = 0, ..., (L-1)\}$, according to the following (general) expression:

$$\hat{\mathbf{\Phi}}_{ML} = \underset{0 \le l \le L-1}{\arg\max} \left\{ z_l \right\}. \tag{19}$$

A. The Decision Statistics for Nakagami-distributed multipath fading

Obviously, the form assumed by the decision statistics $\{z_l\}$ in (19) depends, indeed, on the pdf adopted to model the channel-coefficients $\{h_n(j,i)\}$. Specifically, after indicating as $\sigma_n^2 \triangleq \mathrm{E}\left\{h_n^2(j,i)\right\}$ the average squared amplitude of the n-th path, in the Appendix A it is proved that, when the channel coefficients $\{h_n(j,i)\}$ are zero-mean real-valued uncorrelated Nakagami r.v.s, with assigned fading figure $m \ge 1/2$ (see [26, pp.47-48] for the general properties of the Nakagami *m*-distribution) the corresponding decision statistics in (19) assume the following expression:

$$z_l = \sum_{n=0}^{V} \sum_{j=1}^{N_r} \sum_{i=1}^{N_t} \ln\left\{\cosh\left[\omega_n (\underline{\mathbf{y}}_j(n)^T \underline{\mathbf{e}}_i(l))\right]\right\}$$

$$, l = 0, ..., L-1, \tag{20}$$

where

$$\omega_n \triangleq \beta \sqrt{\frac{4\sigma_n^2}{\sigma_n^2 \beta^2 + 2m}}, \ \ n = 0\,, \ldots, V. \tag{20.1}$$

while $\underline{\mathbf{e}}_i(l)$ is the i-th column of the l-th (matrix) codeword $\mathbf{\Phi}_l$ of the employed STOPPM code (see eq.(14)).

Furthermore, the $(M \times 1)$ column vector $\underline{\mathbf{y}}_j(n)$ in (20) is the n-th column of the previously introduced $(M \times (V+1))$ observation matrix $\mathbf{Y}_j$ (see eq.(11) and related text). So, $\underline{\mathbf{y}}_j(n)$ is related to the transmitted space-time codeword $\mathbf{\Phi}_l$ as in

$$\underline{\mathbf{y}}_j(n) = \beta \mathbf{\Phi}_l \underline{\mathbf{h}}_n(j) + \underline{\mathbf{w}}_j(n), \quad 0 \le n \le V, \;\; 1 \le j \le N_r, \tag{21}$$

where $\underline{\mathbf{h}}_n(j)$ denotes the n-th column of the $(N_t \times N_r)$ j-th channel matrix $\mathbf{H}_j$ composing $\mathbf{H} \triangleq [\mathbf{H}_0 ... \mathbf{H}_V]$ in (11), while $\underline{\mathbf{w}}_j(n)$ is the j-th column of the $(M \times N_r)$ Gaussian noise matrix $\mathbf{W}_j$ constituting the overall noise matrix $\mathbf{W} \triangleq [\mathbf{W}_0 ... \mathbf{W}_V]$ in (11).

B. The Decision Statistics for Gaussian distributed multipath fading

Let the channel amplitude $\alpha_n(j,i)$ in (2) be Gaussian distributed and the corresponding phase $\beta_n(j,i)$ be a binary r.v. with equally distributed outcomes. Thus, by following the same steps reported in the Appendix A for the Nakagami case, it can be proved that the decision statistics in (19) assume the following expression (see also [33, Appendix A]):

$$z_l = \sum_{n=0}^{V} \sum_{j=1}^{N_r} \sum_{i=1}^{N_t} \chi_n (\underline{\mathbf{y}}_j(n)^T \underline{\mathbf{e}}_i(l))^2, \;\; l = 0...L-1, \tag{22}$$

where χ_n is defined as

$$\chi_n \triangleq \left(1 + \frac{1}{\sigma_n^2 \beta^2}\right)^{-1}, \;\; n = 0, \ldots, V, \tag{22.1}$$

C. The Decision Statistics for Nakagami-distributed multipath fading

Finally, let us assume the fading amplitude $\alpha_n(j,i)$ be Log-Normal-distributed. Thus, by carrying out once a time the same basic developments detailed in the Appendix A for the Gaussian case, we arrive at the following expression for the resulting decision statistics (see [33, Appendix E] for the analytical details):

$$z_l = \sum_{n=0}^{V} \sum_{j=1}^{N_r} \sum_{i=1}^{N_t} \ln \left\{ \cosh \left[\varphi_n (\underline{\mathbf{y}}_j(n)^T \underline{\mathbf{e}}_i(l)) \right] \right\}, \quad l = 0, ..., L-1, \tag{23}$$

where φ_n indicates

$$\varphi_n \triangleq \beta e^{c \mu_n}, \;\; n = 0, \ldots, V, \tag{23.1}$$

with $c \triangleq \frac{1}{20} \ln(10)$ and $\mu_n \triangleq \mathrm{E}\{\alpha_n(j,i)\}$.

Remark - On the implementation complexity of the ML Decoder

About actual implementation of the proposed noncoherent ML decoder, eq.(19) suggests a modular architecture composed by L Processor Units (PUs) working in parallel (see Fig.2). Specifically, eqs.(22), (23), (20) point out that the computation of each decision statistic essentially requires $((V+1)N_tN_r)$ summations and products, so that the resulting numerical effort sustained by each PU of Fig.2 over a signalling period is limited up to $O((V+1)N_rN_t)$.

VI. Performance analysis of the proposed transceiver equipped with the STOPPM codes

Since the computation of the WEP $P_E \triangleq P(\hat{\mathbf{\Phi}}_{ML} \neq \mathbf{\Phi})$ of the noncoherent ML decoder in (19) resists to closed-form analytical evaluations, in the next sub-Sections we resort to the Union-Chernoff approach to limit P_E and then acquire insight about the ultimate diversity gains attained by the proposed transceiver equipped with STOPPM codes [34].

A. The Union-Chernoff bound for Nakagami-distributed multipath fading

Let the channel coefficients $\{h_n(j,i)\}$ in (2) be zero-mean uncorrelated *real-valued* Nakagami r.v.s. Thus, in the *Appendix B* it is proved that the Union-Chernoff bound on the corresponding WEP assumes the following (simple) form[4]:

$$P_E \le (L-1) \left(\frac{4e^2 \Gamma(2m)}{\Gamma(m)} \right)^{N_t N_r (V+1)} \cdot \prod_{n=0}^{V} \left[\frac{\left(1 + \frac{\sigma_n^2 \beta^2}{m}\right)}{\left(1 + 2\frac{\sigma_n^2 \beta^2}{m}\right)^2} \right]^{m N_t N_r}, \tag{24}$$

where $\Gamma(.)$ is the (usual) Gamma function [26, pp.47-48]. Thus, since β^2 scales as γ_b, from (24) we conclude that, for large γ_b and $V \ge 1$, the WEP scales as $(\frac{1}{\gamma_b})^{mVN_tN_r}$.

B. The Union-Chernoff bound for Gaussian distributed multipath fading

By performing the same approach developed in the Appendix B for the Nakagami case, we arrive at the following expression for the Union-Chernoff bound when the fading amplitudes are Gaussian distributed (see [33, Appendix.B] for an explicit proof):

$$P_E \le (L-1) \prod_{n=0}^{V} \left[\frac{\left(1 + \sigma_n^2 \beta^2\right)}{\left(1 + \frac{1}{2}\sigma_n^2 \beta^2\right)^2} \right]^{N_t N_r / 2}, \tag{25}$$

Since β^2 in (25) scales as γ_b (see eq.(8)), from (25) we conclude that, for large γ_b and $V \ge 1$, the WEP falls off as $(\frac{1}{\gamma_b})^{VN_tN_r/2}$.

C. The Union-Chernoff bound for Log-normal-distributed multipath fading

Finally, let us consider the fading amplitudes $\{\alpha_n(j,i)\}$ be Log-normal-distributed with fading-parameter $m \ge 1/2$. Thus, for high γ_b the resulting Union-Chernoff bound assumes the following form [33, Appendix D]

$$P_E \le (L-1) \left(\frac{2}{\sqrt{\pi}} \right)^{(V+1)N_tN_r} \prod_{n=0}^{V} \cdot$$

[4] According to eq.(17), the corresponding Union-Chernoff Bound on th Bit-Error-Probability $P_E^{(b)}$ may be obtained by scaling eq.(24) by $L/2(L-1)$.

$$\left[\int_{-\infty}^{+\infty}\exp\left\{-t^2-\beta\varphi_n e^{c\mu_n}\exp\left\{c\sqrt{2}\sigma_r t\right\}\right\}dt\right]^{N_tN_r}, \tag{26}$$

with the term φ_n in (26) given by (23.1) and $\sigma_r \equiv 3.4dB$ (see [36, Table II]). The integral in (26) is known as "Log-normal Frustration Integral" and, unfortunately, it resists closed-form analytical evaluations [14]. However, numerical evaluations we have carried out of this integral lead to the conclusion that, for large γ_b and $V \geq 1$, the bound in (26) falls short as $(\frac{1}{\gamma_b})^{2VN_tN_r}$.

D. Some considerations about the Union-Chernoff limits

Since the real-valued channel coefficients $\{h_n(j,i)\}$ in (2) are assumed to be uncorrelated over *both* the delay-index n and the spatial-indexes (j,i), for $V \geq 1$ the diversity degree offered by the considered (baseband) MIMO UWB-IR channel is of the order of VN_tN_r. Hence, since all the Chernoff bounds in (25), (26), (24) fall short as $\gamma_b^{-kN_tN_r(V)}$ for $V \geq 1$, we conclude that the proposed noncoherent transceiver equipped with STOPPM codes is able to achieve *full-diversity* in the considered multipath-affected communication scenarios. This property generalizes an analogous one previously reported in [4] for the (particular) case of MIMO channels affected by *Gaussian-distributed flat-fading*. Such optimality property retained by the performance of the presented transceiver is also corroborated the numerical results reported in the next Sect.VII.

E. On the performance-effects induced by Poisson-distributed path-arrivals

In principle, the limits reported in (25), (26), (24) should be regarded as Chernoff-bounds *conditioned* on the number V of paths received over a signalling period. Unfortunately, we have experienced that the expectations of these limits over the Poisson-distribution of the r.v. V resists closed-form analytical evaluations, so that, in Sect.VII we resort to numerical methods for evaluating these expectations. However, since for large γ_b all the above reported Chernoff-bounds fall off as $\gamma_b^{-kVN_tN_r}$, we may conclude that, at least for large γ_b, the behavior of the corresponding Poisson-averaged Chernoff-limits is given by

$$\mathrm{E}\left\{\gamma_b^{-kN_rN_tV}\right\} = \exp\left\{-T_s\lambda\left[1-\left(\frac{1}{\gamma_b}\right)^{kN_rN_t}\right]\right\}, \tag{27}$$

where the above expectation is over the Poisson-distribution of the r.v. V (see Note 2). About eq.(27), it should be noted that, since the r.v. V exhibits a non-zero probability to assume the zero-outcome (see Note 2), thus the resulting asymptotical behavior in (27) for the averaged Chernoff-bounds *does not approach zero* for large γ_b, but it presents, indeed, a floor proportional to $e^{-\lambda T_s}$. The numerical plots of Sect.VII confirm, indeed, this asymptotical behavior.

VII. Simulation Setup and Performance Results

To test the performance of the proposed transceiver equipped with STOPPM codes in actual application scenarios, we have carried out several numerical trials. The (unit-energy) pulse $p(t)$ used in all trials is the usual second-time derivative of the Gaussian pulse [1], with shaping factor equal to 0.43ns. Thus, the (effective) duration T_p of the employed pulse is of the order of 1ns [1]. Furthermore, according to [5,6], in the sequel the MIPs of the SISO impulse-responses $\{h_{ji}(t)\}$ in Fig.1 are assumed to fall exponentially off, e.g.,

$$\sigma_n^2 \triangleq \mathrm{E}\left\{h_n^2(j,i)\right\} \equiv$$

$$\begin{cases} 0, & \text{for } V=0, \\ \frac{e^{-\tau_n/\gamma}}{\sum_{k=0}^{V-1}e^{\tau_k/\gamma}}, \quad n=0,\ \ldots,V-1, & \text{for } V\geq 1, \end{cases} \tag{28}$$

where $\gamma(ns)$ in (28) is the power-decay factor of the simulated channel (see the 3-rd column of Table I). Finally, after assuming that the equivalent bandwidth $B_e(Hz)$ of the radiated signals in (1) equates $1/T_p$ [1], directly from (1) it follows that the spectral efficiency η_B of all simulated systems may be directly evaluated according to

$$\eta_B \triangleq \frac{\lg_2 L}{B_eT_s} = \frac{T_p\lg_2 L}{N_f(MT_p+T_\mu)}$$

$$\equiv \frac{\lg_2 L}{N_f(M+T_\mu/T_p)}\ (bit/sec/Hz). \tag{29}$$

In the following sub-sections we evaluate, at first, the performance achieved by the proposed transceiver in terms of BER and coverage-range. Afterwards, we pass to test its performance robustness against the degrading effects induced by IPI, mistiming and spatially-correlated fading. In all the carried out numerical tests, path-arrivals have been generated according to the Poisson-statistic and, then, all the reported numerical results are averaged over the Poisson-statistic of the arrival-times.

A. BER-vs-SNR performance

Main goal of the first set of numerical plots reported in Figs.4,5,6 is to point out the effect of the fading statistics on the BER-v.s.-SNR performance of the proposed transceiver equipped with STOPPM codes. To better appreciate the performance improvements arising from the transmit diversity (e.g., from the utilization of the STOPPM codes at the transmit side), we have (numerically) implemented the Multiple-Input Single-Output (MISO) versions of the proposed transceiver with $N_r = 1$ and $N_t = 1,2,3$. The corresponding SISO impulse-responses $\{h_{ji}(t)\}$ in (2) have been generated according to the CM6 UWB-IR channel model (see Fig.3 and Table I), being fading uncorrelated over both time and spatial dimensions. All the simulated systems work at the same spectral efficiency of $1/200$ (bit/sec/Hz).

An examination of the performance plots of Figs.4,5,6

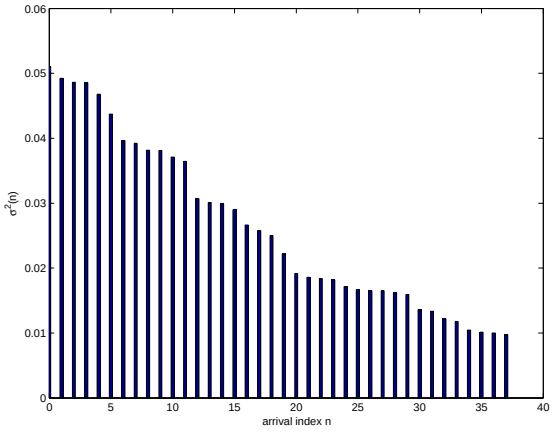

Figure 3. MIP behavior for a CM6, SISO UWB-IR channel [5].

leads to three main conclusions. Firstly, at target BERs of about 10^{-5}, we experience SNR gains of about 1.8dB, 2.5dB, and 2.3dB by passing from $N_t = 1$ to $N_t = 3$ for Log-normal, Nakagami and Gaussian-distributed fading, respectively.

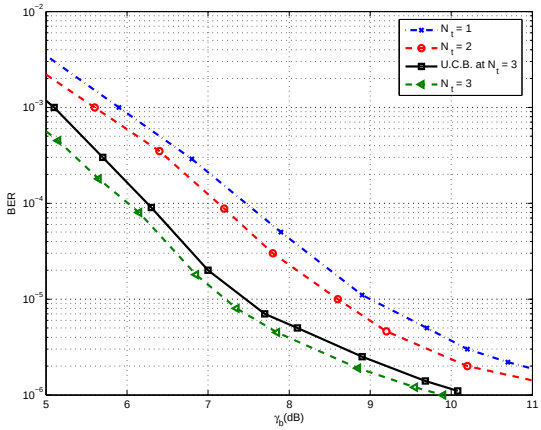

Figure 4. Performance plots of the proposed transceiver equipped with STOPPM codes for Log-normal multipath fading. The number of receive antennas is $N_r = 1$, while the number of frames is $N_f = 8$. The plot marked as $-\blacksquare-$ reports the corresponding Poisson-averaged Union-Chernoff Bound (U.C.B) at $N_t = 3$.

This confirms that the proposed transceiver equipped with STOPPM codes is able to attain noticeable transmit-diversity gains. Second, as predicted by the developed Chernoff-bounds, at SNRs ranging from 5-6dB to 15-16dB, the performance plots of Fig.6 for Gaussian distributed fading are the worst ones, while those of Fig.4 for Log-normal distributed fading are the best ones. This gives evidence to the conclusion that, in terms of BER performance, the Gaussian fading is the most penalizing one. Thirdly, the obtained numerical curves well match the corresponding ones dictated by the (Poisson-averaged) Chernoff-bounds, even at SNRs as low as 7-8dB. In turn, this confirms the optimality (at least in terms of achieved diversity) of the employed STOPPM codes.

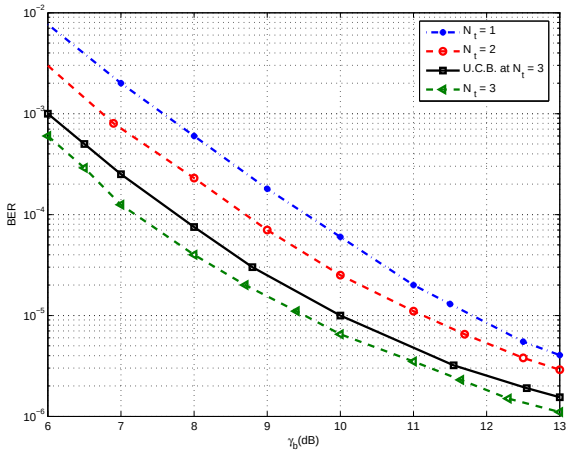

Figure 5. Performance plots of the proposed transceiver equipped with STOPPM codes for Nakagami multipath fading with m=0.8. The number of receive antennas is $N_r = 1$, while the number of frames is $N_f = 8$. The plot marked as $-\blacksquare-$ reports the corresponding Poisson-averaged Union-Chernoff Bound (U.C.B) with $N_t = 3$.

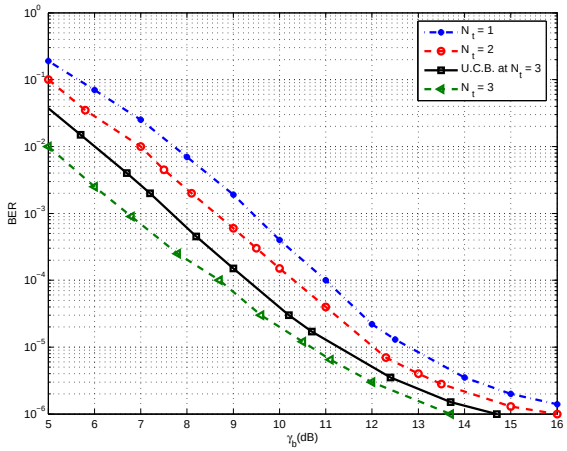

Figure 6. Performance plots of the proposed transceiver equipped with STOPPM codes for Gaussian multipath fading. The number of receive antennas is $N_r = 1$, while the number of frames is $N_f = 8$. The plot marked as $-\blacksquare-$ reports the corresponding Poisson-averaged Union-Chernoff Bound (U.C.B) at $N_t = 3$.

B. Coverage Range extension

The spatio-temporal diversity and coding gain pointed out by the performance plots of Figs.4,5,6 may be turned into corresponding range-extensions, when the transceiver is forced to operate at a target BER. Hence, to test the range-extension capability of the proposed MIMO transceiver, we have implemented several MIMO UWB-IR channels with N_t, N_r ranging from 1 to 3 (see Table II). The SISO impulse responses $\{h_{ji}(t)\}$ composing the simulated MIMO channels have been generated according to the CM5 UWB-IR channel model (see Table I), while the path-loss has been generated according to the Petroff-Siwiak model with $A_{sys} = 1$ and $A_b = 10^{0.68}$ (see eq.(2) of [27]). Furthermore, being focused on NLOS outdoor propagation scenarios, in the carried out tests the transmit power has been set at $2.5mW$, while the fading has been

N_t	N_r	Coverage Ranges (in mt.)
1	1	10
1	2	23
2	2	31
2	3	45
3	3	53

TABLE II.
COVERAGE-RANGES OF MIMO UWB-IR SYSTEMS EQUIPPED WITH STOPPM CODES IN THE PRESENCE OF NAKAGAMI MULTIPATH FADING AND $m = 1.8$.

generated spatially uncorrelated. The throughput of the tested systems is of 136Mbit/sec at a target BER of 10^{-6}.

The obtained coverage ranges are reported in Table II. This last leads to two main conclusions. Firstly, by passing from $N_r = N_t = 1$ (e.g., a SISO system) to $N_r = N_t = 2$, the coverage-range increases of about 2.6 times, while, when we pass from $N_r = N_t = 1$ to $N_r = N_t = 3$, the range-extension factor arises to 4.61. Secondly, the proposed transceiver with $N_t = N_r = 2$ attains coverage-ranges beyond 30mt, thus doing its utilization appealing even for outdoor medium/long-range 4GWLAN-compliant applications.

C. SNR-loss due to IPI

As previously anticipated in Sect.II-B, under IPI-affected operating conditions, the orthogonality property of the transmitted PPM-signals is lost at the receiver side, so that the relationship in (4) is no longer met. This means that, when the IPI effects are not negligible, thus the $\{\phi_i(l)\}$-statistics in (9) are no longer $\{0,1\}$-valued, and, indeed, they may assume any value over the interval [0,1]. By numerical trials, we have tested the robustness of the proposed transceiver against IPI effects for various values of the η-parameter in (5). The tested MIMO links are affected by Gaussian-distributed spatially-uncorrelated multipath fading, and the corresponding SISO impulse responses $\{h_{ji}(t)\}$ are generated according to the CM6 UWB-IR channel model (see Table I). An examination of the performance plots of Fig.7 shows that, at target BERs around 10^{-5}, the IPI-induced SNR loss is limited up to 0.3dB for η values of the order of 0.8, while arises to $1.3dB$ for η values of the order of 0.3[5]. These results support the conclusion that, although the proposed transceiver is designed under the assumption of IPI-free operating conditions, nevertheless, its performance is quite robust against IPI-induced degrading effects.

D. Performance Sensitivity to mistiming effects

To test performance sensitivity of the proposed transceiver to mistiming effects, let us assume that the received analog signals in (3) are affected by a time-offset parameter ε unknown at the receiver-side, so that the signal measured at the output of the j-th receive antenna

[5] $\eta = 0.3$ means that IPI-free operating conditions are guaranteed (only) over 30% of the overall working-time of the transmission system.

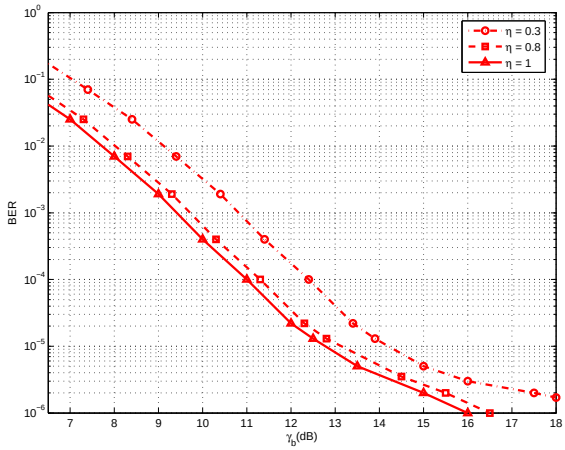

Figure 7. IPI-effects on the performance of the proposed transceiver equipped with STOPPM codes for Gaussian-distributed multipath. The numbers of transmit and receive antennas are $N_t = 2$ and $N_r = 1$ respectively, while the number of frames is $N_f = 8$.

equates

$$y_j(t-\varepsilon) = \sum_{i=1}^{N_t} \sum_{n=0}^{V} h_n(j,i) x^{(i)}(t-\tau_n-\varepsilon) + w_j(t),$$

$$1 \le j \le N_r. \quad (30)$$

In the carried out tests, we have simulated MIMO UWB-IR channels with $N_t = N_r = 2$ transmit/receive antennas affected by spatially-uncorrelated Gaussian fading. The corresponding SISO links $\{h_{ji}(t)\}$ have been generated according to the (strongly scattered) CM5 UWB-IR channel model (see Table I). The numerical plots we obtained are drawn in Fig.8. An examination of these curves points out that, at target BERs of about 10^{-3}, the SNR-loss due to mistiming is limited up to $4.5dB$ when the ratio $\mid \varepsilon/T_p \mid$ is around 8%, while it falls below $1dB$ for values of ratio $\mid \varepsilon/T_p \mid$ limited up to 3%.

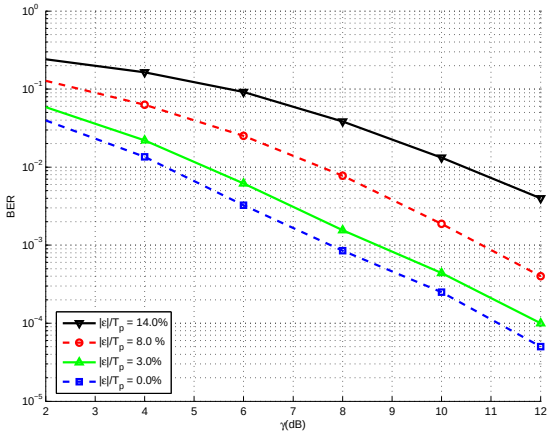

Figure 8. SNR-loss induced by mistiming effects for Gaussian distributed fading.

E. Performance Sensitivity to spatially-correlated fading

Performance robustness of the proposed transceiver against spatially-correlated fading has been numerically evaluated over MIMO UWB-IR channels with path-gains correlated according to the following model:

$$\frac{\mathrm{E}\Big\{h_n(j,i)h_q(l,m)\Big\}}{\sqrt{\sigma_n^2\sigma_q^2}} \equiv \begin{cases} 0, \text{ for } n \neq q \\ 1, \text{ for } n = q \text{ and } j = l \text{ and } i = m \\ c, \text{ otherwise,} \end{cases} \tag{31}$$

where $c \in [-1, 1]$ plays the role of the spatial-correlation coefficient [13]. In the carried out tests, we have simulated MIMO UWB-IR channels equipped with $N_t = N_r = 2$ transmit/receive antennas and affected by Log-normal distributed fading. The impulse-responses $\{h_{ji}(t)\}$ of the underlying SISO UWB-IR links have been generated according to the CM5 channel model (see Table I). Overall, an examination of the resulting performance plots of Fig.9 leads to the conclusion that, at target BERs around 10^{-5}, the SNR-loss induced by spatial-correlation is within $1.4dB$ for values of c as high as 0.6. This

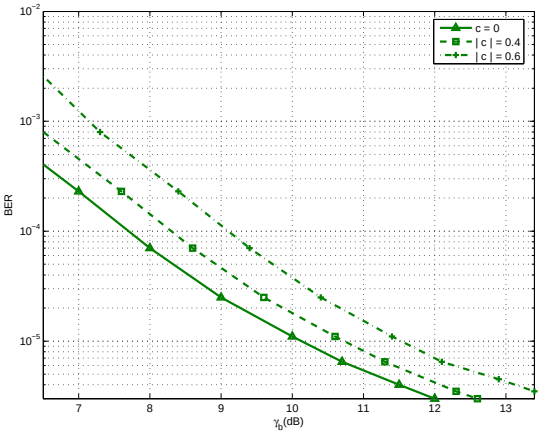

Figure 9. Performance-sensitivity of the proposed transceiver equipped with STOPPM codes on spatially-correlated Nakagami distributed multipath fading. The number of antennas is $N_t = N_r = 2$, while the number of frames is $N_f = 8$.

supports the robustness of the proposed transceiver against spatial-correlation degrading effects.

VIII. Conclusion

In this contribution, we have developed a novel non-coherent transceiver for MIMO UWB-IR applications affected by multipath-fading with Poisson-distributed path-arrivals. The transceiver architecture has been optimized for Nakagami, Gaussian and Log-normal fading, and the resulting performances have been analytically evaluated by developing suitable forms of the Union-Chernoff bound. The carried out analysis points out that, by equipping the proposed transceiver with the recently introduced family of STOPPM codes, the resulting overall communication system is able to attain maximum diversity gain, even in the considered multipath-affected application environments. Furthermore, the analysis of the coverage-ranges achieved by the proposed transceiver supports its utilization even in medium/long-range outdoor 4GWLAN-compliant applications. The carried out numerical tests corroborate the analytical results and point out performance robustness of the transceiver against the degrading effects induced by IPI, spatially-correlated fading and mistiming. The optimized design of (noncoherent) synchronizers for the proposed transceiver able to exploit the diversity offered by the MIMO UWB-IR multipath channel is a companion topic currently under investigation by the Authors [28, Chap.7].

Appendix A
Derivation of the relationship in (20)

The relationship (20) is attained by first evaluating the conditional pdf $p(\mathbf{Y} \mid \mathbf{\Phi}_l, \mathbf{H})$ of the MIMO channel in (11), and then by averaging it over the pdf $p(\mathbf{H})$ of the channel coefficients. Specifically, by considering that all the scalar terms of the noise matrix $\mathbf{W}$ in (11) are mutually-uncorrelated real-valued zero-mean unit-variance Gaussian r.v.s, after conditioning on the transmitted codeword $\mathbf{\Phi}_l$ and channel matrix $\mathbf{H}$, the resulting $(N_r \times V)$ r.v.s in (21) are Gaussian-distributed and mutually uncorrelated. Hence, we may develop the conditional pdf $p(\mathbf{Y} \mid \mathbf{\Phi}_l, \mathbf{H})$ according to the following steps:

$$p(\mathbf{Y} \mid \mathbf{\Phi}_l, \mathbf{H}) = \prod_{j=1}^{N_r}\prod_{n=0}^{V} p(\underline{\mathbf{w}}_j(n) = \underline{\mathbf{y}}_j(n) - \beta\mathbf{\Phi}_l\underline{\mathbf{h}}_n(j))$$

$$\stackrel{(a)}{=} \prod_{j=1}^{N_r}\prod_{n=0}^{V}(2\pi)^{-\frac{M}{2}} \exp\left\{-\frac{1}{2}\underline{\mathbf{y}}_j^T(n)\underline{\mathbf{y}}_j(n) + \beta\underline{\mathbf{y}}_j^T(n)\mathbf{\Phi}_l\underline{\mathbf{h}}_n(j) - \frac{1}{2}\beta^2\underline{\mathbf{h}}_n^T(j)\mathbf{\Phi}_l^T\mathbf{\Phi}_l\underline{\mathbf{h}}_n(j)\right\}$$

$$\stackrel{(b)}{=} (2\pi)^{-\frac{MN_r(V+1)}{2}} \prod_{j=1}^{N_r}\prod_{n=0}^{V} \exp\left\{-\frac{1}{2}\underline{\mathbf{y}}_j^T(n)\underline{\mathbf{y}}_j(n)\right\} \exp\left\{-\frac{1}{2}\beta^2\alpha_n^2(j,i) + \beta\underline{\mathbf{y}}_j^T(n)\mathbf{\Phi}_l\alpha_n(j,i)\beta_n(j,i)\right\}, \tag{A.1}$$

where (a) is due to the Gaussianity of the noise terms, while (b) is given by the Unitary property of the STOPPM codes (see eq.(15)) and by noting that $\underline{\mathbf{h}}_n^T(j)\underline{\mathbf{h}}_n(j) = \sum_{i=1}^{N_t}\alpha_n^2(j,i)$, and $\underline{\mathbf{y}}_j^T(n)\mathbf{\Phi}_l\underline{\mathbf{h}}_n(j) = \sum_{i=1}^{N_t}\underline{\mathbf{y}}_j^T(n)\underline{\mathbf{e}}_i(l)\alpha_n(j,i)\beta_n(j,i)$. Next, let us average the conditional pdf $p(\mathbf{Y} \mid \mathbf{\Phi}_l, \mathbf{H})$ in (A.1) over the channel pdf $p(\mathbf{H})$, according to the following developments:

$$p(\mathbf{Y} \mid \mathbf{\Phi}_l) \triangleq \mathrm{E}\left\{p(\mathbf{Y} \mid \mathbf{\Phi}_l, \mathbf{H})\right\}$$

$$\stackrel{(a)}{=} (2\pi)^{-\frac{MN_r(V+1)}{2}} \left(\frac{2m^m}{\Gamma(m)}\right)^{(V+1)N_tN_r} \prod_{n=0}^{V}\prod_{j=1}^{N_r}\prod_{i=1}^{N_t}\left(\frac{1}{\sigma_n^2}\right)^m \cdot \cdot \exp\left\{-\frac{1}{2N_t}\underline{\mathbf{y}}_j^T(n)\underline{\mathbf{y}}_j(n)\right\} \int_0^{+\infty}\alpha_n^{2m-1}\cdot$$

$$\cdot \exp\left\{-\left(\frac{\beta^2\sigma_n^2+2m}{2\sigma_n^2}\right)\alpha_n^2(j,i)\right\}\cdot$$

$$\cdot \cosh\left(\beta \underline{\mathbf{y}}_j^T(n)\underline{\mathbf{e}}_i(l)\alpha_n(j,i)\right) d\alpha_n(j,i)$$

$$\stackrel{(b)}{=}(2\pi)^{-\frac{MN_r(V+1)}{2}}\left(\frac{2m^m}{\Gamma(m)}\right)^{(V+1)N_tN_r}\prod_{n=0}^{V}\prod_{j=1}^{N_r}\prod_{i=1}^{N_t}\left(\frac{1}{\sigma_n^2}\right)^m\cdot$$

$$\cdot \exp\left\{-\frac{1}{2N_t}\underline{\mathbf{y}}_j^T(n)\underline{\mathbf{y}}_j(n)\right\}\sum_{f=0}^{+\infty}\frac{1}{2f!}\left(\beta \underline{\mathbf{y}}_j^T(n)\underline{\mathbf{e}}_i(l)\right)^{2f}\cdot$$

$$\cdot\int_0^{+\infty}\alpha_n^{2(f+m)-1}\exp\left\{-\left(\frac{\beta^2\sigma_n^2+2m}{2\sigma_n^2}\right)\alpha_n^2(j,i)\right\}d\alpha_n(j,i), \tag{A.2}$$

where, after averaging (A.1) over the $\beta_n(j,i)$-sign pdf of the channel coefficients $h_n(j,i)$, (a) arises from the Nakagami-assumption of the modules $\alpha_n(j,i)$ ($\Gamma()$ is the Gamma function), while (b) is obtained after expressing in power series the $\cosh(.)$ term (see eq.(1.411.1) of [35]). Now, to solve in closed form the integral we have applied the formula 3.462.1 of [35], so to attain the following relationship

$$p(\mathbf{Y}\mid\mathbf{\Phi}_l)=(2\pi)^{-\frac{MN_r(V+1)}{2}}\left(\frac{2m^m}{\Gamma(m)}\right)^{(V+1)N_tN_r}\cdot$$

$$\prod_{n=0}^{V}\prod_{j=1}^{N_r}\prod_{i=1}^{N_t}\left(\frac{4}{\beta^2\sigma_n^2+2m}\right)^m\sum_{f=0}^{+\infty}\frac{1}{2f!}\left(\beta \underline{\mathbf{y}}_j^T(n)\underline{\mathbf{e}}_i(l)\right)^{2f}\cdot$$

$$\left(\sqrt{\frac{4\sigma_n^2}{\sigma^2\beta^2+2m}}\right)^{2f}\exp\left\{-\frac{1}{2N_t}\underline{\mathbf{y}}_j^T(n)\underline{\mathbf{y}}_j(n)\right\}\cdot$$

$$\Gamma\left(2(f+m)\right)D_{-2(f+m)}(0). \tag{A.3}$$

where, $D_p(z)$ is known as "Parabolic Cylinder Function" defined in eq.(9.241.2) of [35]. Now, before proceeding we need to prove the following $Proposition 1$

Proposition 1- Let $\mathbf{\Phi}_l$ and $\mathbf{\Phi}_q$, two distinctive codeword matrices of the STOPPM coding, as defined in (14). If (and only if) the following inequality is met

$$\sum_{f=0}^{+\infty}\frac{1}{2f!}\left(\sqrt{\frac{4\sigma_n^2}{\sigma_n^2\beta^2+2m}}\beta \underline{\mathbf{y}}_j^T(n)\underline{\mathbf{e}}_i(l)\right)^{2f}\geq$$

$$\sum_{f=0}^{+\infty}\frac{1}{2f!}\left(\sqrt{\frac{4\sigma_n^2}{\sigma_n^2\beta^2+2m}}\beta \underline{\mathbf{y}}_j^T(n)\underline{\mathbf{e}}_i(q)\right)^{2f}, \tag{A.4}$$

then we may write the following inequality:

$$\sum_{f=0}^{+\infty}\frac{1}{2f!}\left(\sqrt{\frac{4\sigma_n^2}{\sigma_n^2\beta^2+2m}}\beta \underline{\mathbf{y}}_j^T(n)\underline{\mathbf{e}}_i(l)\right)^{2f}\cdot$$

$$\cdot\Gamma(2(f+m)D_{-2(f+m)}(0)\geq$$

$$\sum_{f=0}^{+\infty}\frac{1}{2f!}\left(\sqrt{\frac{4\sigma_n^2}{\sigma_n^2\beta^2+2m}}\beta \underline{\mathbf{y}}_j^T(n)\underline{\mathbf{e}}_i(q)\right)^{2f}\cdot$$

$$\cdot\Gamma(2(f+m)D_{-2(f+m)}(0) \qquad 0\leq l,q\leq L-1. \tag{A.5}$$

Let (A.4) be met. Since all the arguments into the brackets $()$ do not depend on the f-index we have that

$$\frac{1}{2f!}\left(\sqrt{\frac{4\sigma_n^2}{\sigma_n^2\beta^2+2m}}\beta \underline{\mathbf{y}}_j^T(n)\underline{\mathbf{e}}_i(l)\right)^{2f}$$

$$\geq\frac{1}{2f!}\left(\sqrt{\frac{4\sigma_n^2}{\sigma_n^2\beta^2+2m}}\beta \underline{\mathbf{y}}_j^T(n)\underline{\mathbf{e}}_i(q),\right)^{2f}. \tag{A.6}$$

Now, if we take in (A.6) the summation over f and multiply both members by the not negative (scalar) product $\Gamma(2(f+m))D_{-2(f+m)}(0)$ we directly arrive at the inequality (A.5). ■

The derivation of (A.4) from the inequality (A.5) requires only few (easy) steps we do not report here (see [28, Appendix E] for further details).

The last step we do to arrive at the decision statistics in (20) is to neglect all terms in (A.3) that do not depend from the source index l so to consider them not relevant for the ML detection on the radiated source symbol. Furthermore, after considering the $Proposition 1$ so to individuate only those terms inside the sum over f in (A.3) that are relevant for the ML detection, from (A.3) the corresponding the corresponding Log-likelihood function is expressed as:

$$\ln\left(p\left(\mathbf{Y}\mid\mathbf{\Phi}_l\right)\right)=$$

$$\sum_{n=0}^{V}\sum_{j=1}^{N_r}\sum_{i=1}^{N_t}\left\{+\frac{1}{2}\left(1+\frac{1}{\sigma_n^2\beta^2}\right)^{-1}\left(\underline{\mathbf{y}}_j^T(n)\underline{\mathbf{e}}_i(l)\right)^2\right\}. \tag{A.7}$$

Finally, the maximization of the expression (A.7) leads to the relationships (19) and (20).

By performing similar developments, we obtain the corresponding relationships in (23) and (20) of the decision statistics for Gaussian and Log-normal-distributed fading, respectively. The interested reader may refer to [33, Appendix A, Appendix C]. ■

APPENDIX B
DERIVATION OF THE UNION-CHERNOFF BOUND IN (25)

To derive the expression (24), we resort to the Union-Chernoff bound for upper limiting the Pairwise Error Probabilities (PEPs): $P_{lm}\triangleq P\left(\widehat{\mathbf{\Phi}}_{ML}=\mathbf{\Phi}_l\mid\mathbf{\Phi}=\mathbf{\Phi}_m\right)$, $l\neq m$. We will prove that the considered UWB-IR transceiver of Figs.1,2, equipped with the STOPPM codes, is able to attain the maximum diversity gain. After indicating by $s\geq 0$ the Chernoff-parameter, from eqs.(19), (20) we obtain

$$P_{lm}\equiv P\left\{z_l-z_m\geq 0\mid\mathbf{\Phi}=\mathbf{\Phi}_m\right\}$$

$$\stackrel{(a)}{\leq}\mathrm{E}\left\{\exp\left(s\sum_{n=0}^{V}\sum_{j=1}^{N_r}\sum_{i=1}^{N_t}\ln\left(\frac{\cosh(\omega_n\underline{\mathbf{e}}_i^T(l)\underline{\mathbf{y}}_j(n))}{\cosh(\omega_n\underline{\mathbf{e}}_i^T(m)\underline{\mathbf{y}}_j(n))}\right)\right)\right\}$$

$$\stackrel{(b)}{=} \prod_{n=0}^{V}\prod_{j=1}^{N_r}\prod_{i=1}^{N_t}\left(\mathrm{E}\left\{\cosh(\omega_n \underline{\mathbf{e}}_i^T(l)\underline{\mathbf{w}}_j(n))\right\}\right)^s \cdot$$

$$\left(\mathrm{E}\left\{\mathrm{sech}(\omega_n\beta h_n(j,i)\right\}\right)^s \qquad \text{(B.1)}$$

where (a) is the Chernoff bound on P_{lm} [26], while to arrive at (b) we have considered the following steps: assumed $\mathbf{\Phi}_m$ the codeword matrix actually radiated, the resulting scalar products are $\underline{\mathbf{e}}_i^T(l)\underline{\mathbf{y}}_j(n) = \underline{\mathbf{e}}_i^T(l)\underline{\mathbf{w}}_j(n)$ and $\underline{\mathbf{e}}_i^T(m)\underline{\mathbf{y}}_j(n) = \beta h_n(j,i) + \underline{\mathbf{e}}_i^T(m)\underline{\mathbf{w}}_j(n)$. Moreover, such scalar products composing the arguments of $\cosh(.)$ and $\mathrm{sech}(.) \equiv \frac{1}{\cosh(.)}$ functions in (a), are mutually uncorrelated, due to the Orthogonality property of the STOPPM codes (see eq.(15)). As a consequence, we may separately take the expectations over $\cosh^s(.)$ and $\mathrm{sech}^s(.)$, (e.g., $\mathrm{E}\left\{\exp\left(s\ln(\cosh(.)\mathrm{sech}(.))\right)\right\} = \mathrm{E}\left\{\cosh^s(.)\right\}\mathrm{E}\left\{\mathrm{sech}^s(.)\right\}$). Finally, if we confine the Chernoff s-parameter into the real interval [0,1], the resulting $\cosh^s(.)$ and $\mathrm{sech}^s(.)$ are $\cap$-convex functions, so that we may apply the Jensen inequality [35, pp. 1056] and arrive at (b). Now, let us solve the above two expectations in (B.1), and in this regard let us assume to work under high SNR (e.g., high β) so to approximate the arguments inside the $\mathrm{sech}(.)$ to $\beta h_n(j,i)$. In doing so, after considering the Gaussianity assumption of the noise terms $\underline{w}_j(n)$, we resort formula (3.546.2) of [35] so to attain this following (closed-form) expression

$$\mathrm{E}\left\{\cosh(\omega_n\underline{\mathbf{e}}_i^T(l)\underline{\mathbf{y}}_j(n))\right\} = \frac{2}{\sqrt{\pi}}\int_0^{+\infty}\exp\left(-\omega_n\underline{\mathbf{e}}_i^T(l)\underline{\mathbf{y}}_j(n)\right)^2 \cdot$$

$$\cdot\cosh\left(\omega_n\underline{\mathbf{e}}_i^T(l)\underline{\mathbf{y}}_j(n)\right)d(\underline{\mathbf{e}}_i^T(l)\underline{\mathbf{y}}_j(n)) = \exp\left(-\frac{\omega_n^2}{2}\right) \qquad \text{(B.2)}$$

and after considering the Nakagami assumption of the channel paths $\alpha_n(j,i)$, we attain

$$\mathrm{E}\left\{\mathrm{sech}(\omega_n\beta h_n(j,i)\right\} \equiv \mathrm{E}\left\{\mathrm{sech}(\omega_n\beta\alpha_n(j,i)\right\}$$

$$\stackrel{(a)}{=} \frac{2}{\Gamma(m)}\left(\frac{m}{\sigma_n^2}\right)^m\int_0^{+\infty}\alpha_n^{2m-1}\exp\left(-\frac{m\alpha_n^2(j,i)}{\sigma_n^2}\right)\cdot$$

$$\cdot\mathrm{sech}(\omega_n\beta\alpha_n(j,i))d\alpha_n(j,i)$$

$$\stackrel{(b)}{=} \frac{4}{\Gamma(m)}\left(\frac{m}{\sigma_n^2}\right)^m\sum_{k=0}^{+\infty}\sum_{f=0}^{+\infty}(-1)^k\frac{(-1)^f}{f!}\left(\frac{1}{(2k+1)\beta\omega_n}\right)^{2m}\cdot$$

$$\cdot\left(\frac{m}{\sigma_n^2(\ (2k+1)\beta\omega_n)^2}\right)^f\Gamma(2f+2m)$$

$$\stackrel{(c)}{\approx} \frac{4\Gamma(2m)}{\Gamma(m)}\left(\frac{m}{\sigma_n^2(\beta\omega_n)^2}\right)^m \qquad \text{(B.3)}$$

After expanding in power series $\exp(.)$ and $\mathrm{sech}(.)$ functions, we have applied the formula (1.232.2) of [35] to solve in closed form the integral in (a) and arrive at (b), while after considering only the terms with $f = k = 0$ we have attained the approximated expression in (c). Now, the last steps we follow to arrive at eq.(24) is to replace the expression of ω_n in (B.2) and (B.3). Specifically, under the assumption of high SNR (that is, high β), we may approximate $\exp\left(\frac{\omega_n^2}{2}\right) = \exp\left(\frac{2}{1+\frac{2m}{\sigma_n^2\beta^2}}\right)$ to $\exp(2)$, and $\frac{\beta^2\omega_n^2\sigma_n^2}{m} = \frac{4\sigma_n^2\beta^2}{m\left(1+\frac{2m}{\sigma_n^2\beta^2}\right)}$ to $\frac{4\sigma_n^2\beta^2}{m}$.

Finally, the optimal value s_{opt} of the Chernoff-parameter in (B.1) (e.g., the value of s that minimizes (B.1))) may be directly evaluated by noting that under high SNR values, the expressions (B.2) and (B.3) are less than unit. As a consequence, $s_{opt} = 1$. Hence, after introducing $s = s_{opt} = 1$ into (B.1) , and after considering the expressions (B.2) and (B.3), we finally arrive at eq.(24).

■

REFERENCES

[1] M. Z. Win, R. A. Sholtz, "Ultra Wide Bandwidth Time-Hopping Spread-Spectrum Impulse Radio for Wireless Multiple-Access Communications ", *IEEE Tr. on Comm.*, vol.48, pp. 679-691, Apr. 2000.

[2] L. Yang, G. B. Giannakis, "Space-time Coding for Impulse Radio", *IEEE Conf. on Ultra Wide Band. Syst.*, pp.235-239, 2002.

[3] H. Liu, C. Qiu, Z. Tian, "Error Performance of Pulse-Based Ultra-Wideband MIMO Systems Over Indoor Wireless Channels", *IEEE Trans. on Wireless Comm.*, vol.4, no.6, pp.2939-2944, Nov.2005.

[4] E. Baccarelli, M. Biagi, C. Pelizzoni, N. Cordeschi, "A new family of optimized Orthogonal Space-Times Codes for PPM-based MIMO Systems with Imperfect Channel Estimates", accepted for the pubblication on *Wireless Personal Communications*, Springer, available at http://infocom.uniroma1.it/∼pelcris/WPC07-stoppm.pdf.

[5] A. F. Molisch, D. Cassioli, et Alii, "A Comprehensive Standardized Model for Ultrawideband Propagation Channels", *IEEE Tr. on Antennas and Propagation*, vol.54, no.11, pp.3151-3166, Nov. 2006.

[6] C. W. Kim, X. Sun, L. C. Chiam, "Characterization of Ultra-Wideband Channels for Outdoor Office Environment", *IEEE WCNC 2005*, vol.2, pp. 950-955, Mar. 2005.

[7] M.Weisenhorn, W. Hirt, "Performance of binary antipodal signaling over the indoor MIMO channel", *IEEE Intern. Conf. on Comm. 2003 (ICC'03)*, vol.4, pp.2872-2878, May 2003.

[8] K.Yu, B.Ottersten, "Models for MIMO propagation channels: a review", *Wireless Comm. and Mob. Comp.*, vol.2, pp. 653-666, July 2002.

[9] A.Saleh, R.Valenzuela, "A Statistical Model for indoor Multipath propagation", *IEEE Journ. on Select. Areas in Comm. (JSAC)*, vol.5, no.2, pp.128-137, Feb. 1987.

[10] R.J.M.Cramer, A.Scholtz, M.Z. Win, "Evaluation of an Ultra-Wide-Band propagation Channel", *IEEE Tr. on Antennas and Propagation*, vol.50, no.5, pp.561-570, May 2002.

[11] X.Cheng, W.Zhu, "A Subspace Method Detection of Analog Space-Time Codes for Multi-Antenna Ultra-Wideband Transmissions", *IEEE Comm. Lett.*, vol. 9, no.6, pp. 493-495, June 2005.

[12] W.Siriwongpairat, M.Olfait, K.J. Liu "On the Performance Evaluation of TH and TH UWB MIMO Systems", *Proc. of IEEE WCNC' 04*, vol.3, March 21-25, pp.1800-1805, Mar.2004.

[13] J.H.Reed, et Alii, An introduction to Ultra Wide Band Communication Systems, Ed. Prentice Hall, 2005.

[14] S.Haas, J.H.Shapiro, "Space Time Codes for Wireless Optical Communications", *Eurasip Journal on Applied Signal Processing*, vol.2, no.3, pp. 211-220, Mar. 2002.
[15] J.M.Cramer, R.A.Scholtz, M.Z.Win, "Spatio-Temporal Diversity in Ultra-Wideband Radio", *IEEE Wireleless Comm. and Networking Conf.* (WCNC) 1999, vol.2, pp.888-892, Sept. 1999.
[16] C.Prettie, D.Cheung, L.Rusch, M.Ho, "Spatial Correlation in a Home Environment", *IEEE Conf. on Ultra Wideband Syst. and Tech.*, pp.65-69, May 2002.
[17] Y.Ishiyama, T.Ohtsuki, "Performance Comparison of UWB-IR using Rake Receivers in UWB channel Models", *IEEE Ultra Wideband Syst. 2004*, pp. 226-230, May 2004.
[18] L.Zhiwei, B.Prekumar, A.S.Madhukumar "MMSE Detection for High Data Rate UWB MIMO Systems", *IEEE Vehic. Tech. Conf.*, vol. 2, pp. 1463-1467, Sept. 2004.
[19] L.Yang, G.B.Giannakis, "Analog Space-Time Coding for Multiantenna Ultra-Wideband Transmissions", *IEEE Trans. on Comm.*, vol.52, no.3, pp.507-517, Mar.2004.
[20] T. Ezaki, T.Ohtsuki, "Performance Evaluation of Space Hopping Ultra Wideband Impulse Radio (SH-UWB-IR) System", *IEEE Intern. Conf. on Comm. 2004 (ICC'04)*, Paris 20-24 June, vol.6, pp.3591-3595, June 2004.
[21] T. Ezaki, T.Ohtsuki, "Diversity Gain in Ultra Wideband Impulse Radio (UWB-IR)", *IEEE Conf. on Ultra Wideband Syst. and Tech.*, 16-19 November, pp.56-60, Nov. 2003.
[22] E.Baccarelli, M.Biagi, R.Bruno, M.Conti, E.Gregori, "Broadband Wireless Access networks: a Roadmap on Emerging Trends and Standards", *in Broadband Services: Business Model and Tech. for Community Networks*, pp.215-240, Wiley, 2005.
[23] J.C.Guey, M.P.Fitz, M.R.Bell, W.Y.Kuo, "Signal Design for transmitter diversity wireless communication systems over Rayleigh fading channels", *IEEE Trans. on Comm.*, vol. 47, no.4, pp. 527-537, Apr. 1999.
[24] S. Tan, B. Kannan, and A. Nallanathan, "Performance of UWB multiple access impulse radio systems in multipath environment with antenna array", in *Proc. IEEE Global Telecommunications (GLOBECOM)*, San Francisco, CA, vol. 4, pp. 2182-2186, Dec. 2003.
[25] E.Baccarelli, M.Biagi, C.Pelizzoni, N.Cordeschi, "Multi-Antenna Noncoherent ML Synchronization for UWB-IR faded channels" *Journal of Communications and Networks (JCN)*, vol. 8, no.2, pp. 194-204, June 2006.
[26] J.Proakis, Digital Communications, Ed.4 McGrawHill, 2001.
[27] K.Siwiak, A.Petroff, "A Path link model for Ultra Wide Band Pulse Transmissions", *IEEE VTC2001*, Rhodes, Greek, May 2001.
[28] C.Pelizzoni, A novel Multi-Antenna Platform based on UWB-IR technolgy for emerging 4GWLANs, Phd. Thesis, available at http://infocom.uniroma1.it/ $\sim$ pelcris/thesis.pdf, 2007.
[29] V.V.S Nagesh Polu, B.G. Colpits, B.R. Peterson, "Symbol-wavelength MMSE gain in a multi-antenna UWB system", *IEEE Proc. of the 4-th Annual Communication Networks and Services Research Conference (CNSR'06)*, pp.1-5, May 2006.
[30] A.Parihar, L.Lampe, R.Schober, C.Leung, "Equalization for 4BOK DS-UWB Systems", *IEEE Intern. Conf. on Comm. 2006 (ICC'06)*, Vol.4, pp.1482-1487, June 2006.
[31] H.Wymeersch, G.Zussman, M.Z.Win, "SNR Analysis for Multi-Rate UWB-IR", *IEEE Communication Letters*, vol.11, no.1, pp.49-51, Jan. 2007.
[32] B.M.Hochwald, T.L. Marzetta, "Unitary space-time modulation for Multiple-Antenna communications in Rayleigh flat fading", *IEEE Transactions on Inform. Theory*, Vol.46, no. 2, pp.543-564, March 2000.
[33] E. Baccarelli, M. Biagi, C. Pelizzoni, N. Cordeschi, "Noncoherent Transceivers for multipath-affected MIMO UWB-IR Communications", INFOCOM Tech. Rep., available at http://infocom.uniroma1.it/$\sim$ pelcris/tech.1.pdf
[34] E.Baccarelli, M.Biagi, C.Pelizzoni, N.Cordeschi, "PPM-based Orthogonal Space-Time coding for IR-UWB MIMO channels affected by Poisson-distributed Multipaths", *IEEE International Symposium on Wireless Pervasive Computing (ISWPC) 2007*, Puerto Rico, February 5-7 2007, pp.206-211, Feb.2007.
[35] I.S.Gradshtein, I.M.Ryzhik, Table of Integrals, Series, and Products (Sixth Edition), Academic Press, 2000.
[36] A. F. Molisch, J. R. Foerster, M. Pendergrass, "Channel Models for Ultrawideband Personal Area Networks", *IEEE Wireless Communications*, vol.10, no.6, pp.14-21, Dec. 2003.

Enzo Baccarelli received the Laurea degree (summa cum laude) in electronic engineering and Ph.D. degree in Communication Theory and Systems, both from the "La Sapienza" University of Rome, (Italy), in 1989 and 1992, respectively. In 1995, he received the Post-Doctorate degree in Information Theory and Applications from INFOCOM Department of the "La Sapienza" University, where he also served as Research Scientist from 1996 to 1998. Since 2003 he is full Professor in Telecommunication. He is author of more than 100 international IEEE publications, and he is an Associate Editor of IEEE Communication Letters.

Mauro Biagi was born in Rome in 1974. He received his "Laurea degree" in Telecommunication Engineering in 2001 from "La Sapienza" University of Rome. His research is focused on Wireless Communications (e.g., Multiple Antenna systems and Ultra Wide Band transmission technology), mainly dealing with space-time coding techniques and power allocation/ interference suppression in MIMO-ad-hoc networks. Concerning UWB, his interests focus on transceiver design and UWB-MIMO applications. Since 2006, he' s researcher at the INFO-COM Dept. of "Sapienza" University of Rome.

Cristian Pelizzoni was born in Rome, Italy, in 1977. He received the Laurea Degree in Telecommunication Engineering from "La Sapienza" University of Rome in 2003. He received the Ph.D at the beginning of 2007 in Information and Communication Engineering at the Engineering Faculty of the "Sapienza" University. Currently, he works as contractor researcher at the INFOCOM Dept. of the Engineering Faculty of the "Sapienza" University. His research areas Space-Time coding for wireless channels affected by multipath fading like UWB channels.

Nicola Cordeschi was born in Rome, Italy, in 1978. He received the Laurea degree (summa cum laude) in Telecommunication Engineering in 2004 from " Sapienza" University of Rome. He is pursuing the Ph.D. at the INFO-COM Department of the Engineering Faculty of "Sapienza" University. His research activity focuses on the design and optimization of high performance transmission systems for MIMO wireless content delivery networks.